BVES Regulates Intestinal Stem Cell Programs and Intestinal Crypt Viability after Radiation

Running Title: BVES Regulates Intestinal Stem Cell Programs

Vishruth K. Reddy[1,2,3], Sarah P. Short[1,2], Caitlyn W. Barrett[4], Mukul K. Mittal[1], Cody E. Keating[1], Joshua J. Thompson[1], Elizabeth I. Harris[5], Frank Revetta[5], David M. Bader[1], Thomas Brand[6], M. Kay Washington[5], Christopher S. Williams[1,2,7,8]

[1]Department of Medicine, Vanderbilt University School of Medicine, [2]Department of Cancer Biology, Vanderbilt University School of Medicine, [3]Medical Scientist Training Program, Vanderbilt University School of Medicine, *[4]Department of Neurology, University of Pittsburgh School of Medicine, [5]Department of Pathology, Microbiology, and Immunology, Vanderbilt University School of Medicine, [6]Developmental Dynamics, Heart Science Centre, Imperial College London, [7]Vanderbilt-Ingram Cancer Center, Vanderbilt University Medical Center, [8]Veterans Affairs Tennessee Valley Health Care System, Nashville, TN, USA*

Corresponding Author
Christopher S. Williams, M.D., Ph.D.
Associate Professor of Medicine/Gastroenterology
Associate Professor of Cancer Biology
Director, Physician Scientist Training Program
Vanderbilt University School of Medicine
2231 Garland Ave, 1065D MRB-IV, Nashville, TN 37235-0654
(615) 322-3642; Fax (615) 343-6229
E-mail: christopher.s.williams@vanderbilt.edu

There are no conflicts of interest to disclose

Keywords: BVES, stem cells, radiation enteritis, Wnt signaling, radiation biology

Conception and design: VKR, CSW; Financial support: VKR, CSW, MKW; Administrative Support: VKR; Provision of study material: VKR, SPS, CWB, FR, DMB, TB, MKW, CSW; Collection and/or assembly of data: VKR, SPS, CWB, MKM, CEK, JJT, EIH, FR, DMB, TB, MKW, CSW; Data analysis and interpretation: VKR, SPS, CWB, EIH, FR, DMB, TB, MKW, CSW; Manuscript writing: VKR, SPS, CWB, CSW; Final approval of manuscript: VKR, SPS, CWB, MKM, CEK, JJT, EIH, FR, DMB, TB, MKW, CSW.

Abstract: (250 words)

Blood Vessel Epicardial Substance (BVES/Popdc1) is a junctional-associated transmembrane protein that is underexpressed in a number of malignancies and regulates epithelial-to-mesenchymal transition. We previously identified a role for BVES in regulation of the Wnt pathway, a modulator of intestinal stem cell programs, but its role in small intestinal (SI) biology remains unexplored. We hypothesized that BVES influences intestinal stem cell programs and is critical to SI homeostasis after radiation injury. At baseline, *Bves*$^{-/-}$ mice demonstrated increased crypt height, as well as elevated proliferation and expression of the stem cell marker *Lgr5* compared to wildtype (WT) mice. Intercross with Lgr5-EGFP reporter mice confirmed expansion of the stem cell compartment in *Bves*$^{-/-}$ mice. To examine stem cell function after BVES deletion, we employed *ex vivo* 3D-enteroid cultures. *Bves*$^{-/-}$ enteroids demonstrated increased stemness compared to WT, when examining parameters such as plating efficiency, stem spheroid formation, and retention of peripheral cystic structures. Furthermore, we observed increased proliferation, expression of crypt-base columnar "CBC" and "+4" stem cell markers, amplified Wnt signaling, and responsiveness to Wnt activation in the *Bves*$^{-/-}$ enteroids. *Bves* expression was downregulated after radiation in WT mice. Moreover, after radiation, *Bves*$^{-/-}$ mice demonstrated significantly greater small intestinal crypt viability, proliferation, and amplified Wnt signaling in comparison to WT mice. *Bves*$^{-/-}$ mice also demonstrated elevations in *Lgr5* and *Ascl2* expression, and putative damage-responsive stem cell populations marked by *Bmi1* and *TERT.* Therefore, BVES is a key regulator of intestinal stem cell programs and mucosal homeostasis.

INTRODUCTION

The intestinal epithelium is a rapidly proliferating tissue that is thought to renew itself every 5 days[1,2]. Intestinal homeostasis is maintained by dynamic stem cell populations that reside in invaginations of the intestinal epithelium known as crypts[1,3,4]. Until recently, thorough characterization of these stem cell populations has remained challenging due to the absence of specific markers and suitable methodologies for their identification[1,5]. However, recently-discovered adult intestinal stem cell markers, and recently-developed lineage tracing technologies and innovative *ex vivo* 3D crypt cultures or "enteroid" systems have greatly facilitated their characterization[1,6–8].

Current evidence suggests the existence of ≥2 intestinal stem cell (**ISC**) populations: (1) a rapidly-cycling, crypt-based columnar (**CBC**) stem cell population at the base of the intestinal crypts, whose markers include Lgr5, a transmembrane receptor for R-spondin that amplifies Wnt tone, as well as Ascl2, Olfm4, Msi1, Smoc2, and Sox9; and (2) a more slowly-cycling, quiescent "+4" stem cell population that resides primarily at the +4 position from the base of the crypt and is marked by Bmi1, TERT, Lrig1, and Hopx[1,5,9–11]. Wnt signaling, which regulates numerous biological processes ranging from development to malignancy, is known to be one of the many signaling pathways that governs intestinal homeostasis and is critical to the maintenance of the intestinal stem cell niche[3,12–15]. Intestinal stem cells give rise to daughter cells whose fate is influenced by the Notch pathway, a governor of differentiation programs that regulate intestinal epithelial cell fate. Crosstalk between the Wnt and Notch pathways is known to be critical to differentiation and lineage allocation in the intestine[3,16].

Small intestinal (SI) regenerative responses are often assessed via radiation injury modeling due to the sensitivity of intestinal stem cell populations to ionizing radiation[17–21]. Successful intestinal tissue recovery and regeneration after radiation is mediated by the survival of a subset of stem cells which reconstitute the injured crypt-villus unit[20,21]. The contribution of $Lgr5^{+}$-CBC versus +4-ISC to normal intestinal epithelial renewal and repair after injury is still under debate, but a number of studies have identified a role for each in restoring epithelial integrity after injury[17,18,22,23].

Blood Vessel Epicardial Substance (BVES/Popdc1) is a junctional-associated, three-pass transmembrane protein that was originally isolated from a cDNA screen of the developing heart[24,25]. BVES is highly expressed in epithelial tissues and regulates epithelial-to-mesenchymal transition (EMT)[24,26–31]. We have previously demonstrated that BVES regulates colonic epithelial phenotypes *in vitro* and is a regulator of the Wnt pathway through stabilization of E-cadherin and alterations in β-catenin subcellular localization[26]. As the Wnt pathway is a critical regulator of small intestinal stem cell programs[3,12], we hypothesized that BVES influences intestinal stem cell signaling and is critical to SI homeostasis after radiation injury.

In the present study, we have identified BVES as a key modulator of intestinal epithelial stem cell programs and epithelial regeneration after radiation-induced injury. At baseline, *Bves*$^{-/-}$ mice exhibited higher proliferation, greater crypt depth, and an expanded crypt stem cell compartment. *Ex vivo* 3D-enteroid cultures of *Bves*$^{-/-}$ crypts demonstrated increased stemness, when examined by parameters such as plating efficiency, stem spheroid formation, and retention of peripheral cystic structures. This was accompanied by increased proliferation and expression of CBC rapidly-cycling

stem cell markers, +4 stem cell markers, amplified Wnt signaling, and responsiveness to Wnt activation. Furthermore, we found that *Bves* expression is downregulated in response to radiation in wildtype (WT) mice, and that this downregulation is biologically relevant, as *Bves*$^{-/-}$ mice are protected from radiation-induced injury and demonstrate greater crypt viability, more active stem cell populations, and amplified Wnt signaling after radiation. Finally, enteroids cultured from *Bves*$^{-/-}$ crypts after radiation demonstrated greater plating efficiency, indicating an epithelial tissue-autonomous role for BVES in modulating intestinal crypt viability. Results from these studies suggest that BVES regulates intestinal stem cell signaling and intestinal crypt viability after radiation and that it may serve as a predictive biomarker for patients undergoing radiotherapy.

MATERIAL AND METHODS

Mouse Models

WT (C57BL/6 background) were obtained from the Jackson Laboratories. *Bves*$^{-/-}$ mice have been described in detail[27]. Lgr5-EGFP-ires-CreERT2 mice[8] (The Jackson Laboratory, Bar Harbor, ME) were obtained from R. Coffey (Vanderbilt University). All experiments were performed with 8 to 10 week old male and female mice on C57BL/6 background under guidelines approved by the Vanderbilt Institutional Animal Care and Use Committee (IACUC).

γ-Irradiation Protocol

WT and *Bves*$^{-/-}$ mice were placed in a plexiglass-partitioning device and onto a turntable delivery platform, ensuring uniform radiation dosing of all mice. WT and *Bves*$^{-/-}$ mice received 12 Gy whole-body radiation (WBR) from a Mark I ^{137}Cs source delivered at 1.58 Gy/min. Ninety-three hours after radiation, mice were injected with 0.02 mg/kg of vincristine sulfate (Sigma-Aldrich, St. Louis, MO) to arrest cells in metaphase and facilitate identification of regenerative crypts[19,32]. Mice were euthanized three hours later at the ninety-six hour time point to examine crypt regeneration in the small intestine and colon[32,33]. In a separate experiment, to assess *ex vivo* crypt viability after radiation, WT and *Bves*$^{-/-}$ mice were sacrificed four hours after 12 Gy radiation, with small intestinal crypts harvested and plated for enteroid cultures[32].

Small Intestinal Organoid (Enteroid) Cultures

The crypt-enteroid culture method was modified from Sato et al[6,34]. Six centimeters of the proximal small intestine was dissected, flushed with ice cold

phosphate buffered saline (PBS), dissected into 1 cm pieces, suspended in 5 mL ice cold PBS, and vortexed for 3 seconds. PBS was removed with a pipettor, and the wash was repeated. Tissue was transferred to 5 mL chelation buffer (1mM ethylenediaminetetraacetic acid (EDTA)), made fresh in Dulbecco's phosphate buffered saline (DPBS) and rocked for 10 minutes at 4°C prior to washing twice with 10 mL PBS. 5 mL PBS was added, and the tissue was then shaken gently for 2 minutes. The supernatant was removed, 5 mL PBS was added, and the tissue was again gently shaken for 2 minutes. Supernatant was then decanted. 5 mL fresh chelation buffer was added and chelation was performed for 10 minutes at 4°C with gentle rocking. Crypts were filtered through a 70 μm filter into a pre-chilled 50 mL tube. The filter was rinsed with 5 mL cold shaking buffer (PBS with 43.3mM sucrose and 54.9mM Sorbitol). Complete crypts were counted and enough volume of shaking buffer was transferred for 1200 crypts to a pre-chilled 5 mL round-bottomed tube. Crypts were centrifuged at 150 x g for 10 minutes at 4°C. Shaking buffer was aspirated and crypts were resuspended in 50 μl of Matrigel (BD Bioscience, San Jose, CA, USA), per well, supplemented with 50 ng/mL EGF (R&D Systems, Minneapolis, MN, USA), 100 ng/mL Noggin (R&D Systems), and 500 ng/mL R-Spondin (R&D Systems) unless otherwise specified for growth factor depletion experiments. 50 μg/mL Wnt3a (Millipore, Billerica, MA, USA) was added per well for Wnt3a supplementation experiments. Matrigel was overlayed with 500 μl Minigut culture media (Advanced DMEM/F12 (Invitrogen, Carlsbad, CA, USA)), L-Glutamine (Invitrogen), Penicillin-Streptomycin (Invitrogen), HEPES (Mediatech), N2 Supplement (R&D Systems), B27 Supplement (Invitrogen) and growth factors. Every 4 days, media was replaced with fresh Minigut media. Plating efficiencies

were calculated by dividing the total number of enterospheres formed by the original number of crypts plated at Day 0 and multiplying by 100. Enterospheres were visualized and counted at 24 and 48 hours after plating. Experiments were performed in triplicate and repeated two times. Crypt and villus-enriched epithelial populations for investigation of *Bves* expression were obtained by identical dissociation methods utilized for enteroid cultures, with crypts isolated by filtration through a 70 μm filter.

Immunohistochemistry and Immunofluorescence Staining

At time of sacrifice, small intestines were removed, rinsed with phosphate-buffered saline (PBS), and Swiss-rolled for histological assessment. The tissues were fixed in 10% formalin overnight and transferred to 70% ethanol. Tissues were submitted to Vanderbilt Tissue Processing Shared Resource (TPSR) core for processing and paraffin embedding. For immunohistochemistry (IHC), five micrometer sections were cut, dewaxed, hydrated, and endogenous peroxidase activity quenched with 0.03% hydrogen peroxide in MeOH[35,36]. Antigen retrieval was conducted using Antigen Unmasking Reagent (Vector Laboratories, Burlingame, California, USA) according to manufacturer's instructions. After blocking, primary antibody was added overnight at 4°C. Isotype-matched antibodies were used as negative controls on serial sections. The Vectastain ABC Elite System (Vector Laboratories) was used to visualize staining for immunohistochemistry. Proliferation was measured using anti-phospho-Histone H3 (pH3) Ser10 antibody (Millipore) that labels cells in the mitotic (M) phase of the cell cycle at 1:150 dilution. Enteroendocrine cells were assessed by Chromogranin A (CgA) staining using anti-CgA at 1:1000 (ImmunoStar Inc., Hudson, WI). Anti-lysozyme antibody (Dako, Carpentaria, CA) at 1:500 was utilized to identify Paneth cells. Goblet

cells were identified by Periodic Acid Schiff (PAS) staining. Identification of apoptotic cells was conducted using the ApopTag Plus Peroxidase In Situ Apoptosis Kit (Millipore) according to the manufacturer's protocol. For GFP immunofluorescence (IF) staining, anti-GFP (Novus, Littleton, CO) at 1:500 was utilized, and slides were counterstained and mounted with ProLong Gold antifade including 4′,6-diamidino-2-phenylindole (Invitrogen). Crypt proliferation, Paneth cell quantification, and GFP^+ cell counts was generated by counting cells in 40 sequential, well-aligned crypts from the proximal small intestine. This is presented as the mean number of positive cells per crypt. Crypt apoptosis, enteroendocrine cell counts, and goblet cell counts were obtained by counting cells in 40 sequential, well-aligned crypts and adjacent villi from the proximal small intestine. This is presented as the mean number of positive cells per crypt-villus unit.

Immunoprecipitation and Western blotting

Immunoprecipitations and western blot protocols were carried out as previously described[26]. Briefly, for immunoprecipitation assays, cells were grown in 100-mm cell culture dishes. Once 80-90% confluence was reached, cells were rinsed with ice-cold PBS and incubated for 15 min at 4°C in 1 mL of cell lysis buffer (Sigma) containing 1X phosphatase inhibitor cocktails 2 and 3 (Sigma) and 1X protease Inhibitor cocktail (Sigma). Samples were sonicated for 10 seconds at 4°C. Cellular debris was removed by centrifugation; protein concentration was measured by Bradford method. For immunoprecipitation, approximately 1 mg of total protein was incubated with 2 µg of the respective antibodies (β-catenin: BD Bioscience; BVES: Sigma; IgG: Cell Signaling) overnight at 4°C followed by a 3 hour incubation with 25 □L of protein A/G magnetic

beads (Millipore). The immunoprecipitates were collected by magnetic separation and washed three times with 500 µL of cell lysis buffer. Washed beads were suspended in 50 µL of 2X Laemmli buffer and samples were resolved on 8% SDS-PAGE gel and probed with E-cadherin antibody (BD Bioscience).

RT-PCR analysis

RNA from *Bves*$^{-/-}$ or WT proximal small intestine was isolated using the RNeasy Mini Kit (Qiagen, Valencia, Santa Clarita, California, USA). 20 µl of cDNA was synthesized using the iScript cDNA synthesis kit (Bio-rad, Hercules, California, USA) from 1 µg of total RNA. 1 µl of cDNA was used as a template in each subsequent PCR reaction. SYBR green qRT-PCR was performed using mouse Wnt signaling primer library I (Cat #: MWNT-I), as well as *Lgr5, Ascl2*, *Axin2*, and *PCNA* primers obtained from RealTimePrimers.com according to manufacturer's instructions. Sequences for validated primers for *Lrig1*, *Bmi1*, *Tert, Olfm4, Nanog, Muc2*, *Math1/Atoh1*, *Spedf, JAG1, Hes1, Gfi1,* and *Bves* were obtained from Harvard Primer Bank (Cambridge, MA) and SYBR green qRT-PCR was performed according to manufacturer's instructions (Invitrogen). Expression was analyzed using the delta-delta Ct method and normalized to Glyceraldehyde 3-phosphate dehydrogenase (*Gapdh*).

Statistical Methods

Analyses comparing two groups were analyzed using the Student's *t*-test. One-way ANOVA and Newman-Keuls post-test was used to compare multiple groups. Data is presented as the mean +/- the standard error of the mean (SEM) in bar graphs and a line identifying the mean is shown when all data points are plotted. All of these analyses

were performed using GraphPad Prism®6.0c (San Diego, CA, USA). A $P<0.05$ was considered statistically significant.

RESULTS

BVES regulates intestinal crypt homeostasis.

Previous studies have demonstrated that BVES regulates colonic epithelial phenotypes *in vitro* and Wnt signaling through alterations in β-catenin subcellular localization[26]. However, its role in small intestinal biology and the impact of its deletion *in vivo* on SI homeostasis was not previously examined. To determine if BVES deletion alters crypt morphology, proliferation, or differentiation in the small intestine, we performed histological characterization of *Bves*$^{-/-}$ mice and examined the proximal small intestine. While villus height was comparable to that of WT mice, *Bves*$^{-/-}$ mice demonstrated significantly greater crypt depth (**Figure 1A).** Analysis of crypt dynamics revealed no differences in apoptosis (**Figure 1B, Supplemental Figure 1A**); however proliferation, as measured by phospho-histone H3 IHC, was increased in *Bves*$^{-/-}$ mice (**Figure 1C, S1A**). Additionally, the number of PAS-labeled goblet cells was increased compared to WT mice **(Figure 1D, S1A),** although there were no differences in numbers of Paneth (**Figure 1E, S1A**) or enteroendocrine cells (**Figure 1F, S1A**). These data demonstrate that BVES regulates proliferation, intestinal lineage allocation, and crypt morphology, indicating a previously unrecognized role for BVES in regulating intestinal homeostasis.

BVES modulates intestinal stem cell dynamics.

As stem cell programs and Wnt pathway activation are critical in regulating intestinal homeostasis, we investigated expression of Wnt targets and intestinal stem cell markers in the *Bves*$^{-/-}$ intestine. Transcript levels of *Axin2* were significantly

elevated at baseline in the *Bves*$^{-/-}$ SI (**Figure 2A**). Additionally, we found significant elevation in expression of *Lgr5,* a marker of CBC stem cells and another well-defined Wnt target in the *Bves*$^{-/-}$ SI (**Figure 2B**). There were trending increases in expression of *Lrig1* and *Bmi1*, markers of +4 more slow-cycling stem cell populations (**Figure 2C**). To confirm that BVES loss may be driving the expansion of crypt base columnar stem cell populations, we crossed WT and *Bves*$^{-/-}$ mice with a Lgr5-EGFP reporter line[8], which demonstrated an almost 2-fold increase in the number of GFP^{+} cells/$^{+}$crypt in the *Bves*$^{-/-}$ cohort compared to WT **(Figure 2D)**.

To further interrogate the role of BVES in SI stem cell behavior in an epithelial tissue-autonomous manner, we decided to employ the enteroid modeling system using *ex vivo* cultures of WT and BVES null crypts. Enteroids derived from *Bves*$^{-/-}$ mice demonstrated increased proliferation as determined by *PCNA* expression when harvested 5 days after plating **(Figure 3A)**. *Bves*$^{-/-}$ mice also demonstrated a 3-fold elevation in *Muc2* expression 96 hours after plating **(Figure 3B)**. Thus, the enteroid platform accurately recapitulated observed *in vivo* phenotypes. Because of an elevation in *Muc2* and *Spedf* expression **(Figure S2A)** in the *Bves*$^{-/-}$ enteroids, and the expansion of goblet cells in the *Bves*$^{-/-}$ SI, we investigated expression of Notch targets in SI tissue and enteroids. Interestingly, while we found no differences in expression of Notch signaling genes in small intestinal tissue **(Figure S2C)**, we found significant elevation of *Atoh1* in the *Bves*$^{-/-}$ enteroids **(Figure S2B)**, consistent with our findings of an expanded goblet cell lineage in the *Bves*$^{-/-}$ intestine and suggestive of more pronounced suppression of global Notch signaling in this epithelial-autonomous setting.

The enteroid platform is ideal for testing stem cell function[6,11,37]. The "stemness" of an enteroid can be measured by several growth parameters. For instance, augmented stem cell survival can be measured by an increase in the number of crypts that survive plating when considering the total number of crypts plated and is represented as the plating efficiency. Additionally, percentages of cystic, stem-spheroid structures at specific time points can also serve as a marker for stemness. *Bves*$^{-/-}$ enteroids demonstrated higher plating efficiency **(Figure 3C)** and increased frequency of stem spheroids **(Figure 3D)** at 24 and 48 hours post-plating. After repassaging and maintenance in culture, *Bves*$^{-/-}$ enteroids consistently retained a significantly higher proportion of peripheral cystic structures in comparison to WT enteroids 5 days after passaging **(Figure 3E)**. Lastly, culturing of Lgr5-EGFP-ires-CreERT2 WT and *Bves*$^{-/-}$ enteroids after flow-sorting and plating Lgr5^{+}-GFP^{+} cells demonstrated no significant differences in single-cell plating efficiency (Data not shown), suggesting that this metric of stem cell function is not influenced by loss of BVES and that BVES's effect on stem cell features requires cooperation from other cell populations.

To investigate if these stemness phenotypes corresponded to expansion of stem cell populations, we surveyed for expression of stem cell markers. Both CBC **(Figure 4A)** and +4 stem cell populations **(Figure 4B)** were significantly elevated in the *Bves*$^{-/-}$ enteroids. Additionally, we observed a significant upregulation of Wnt ligands (*Wnt2*, *Wnt2b*, *Wnt3*, *Wnt7a*, *Wnt8B*), Frizzled receptors, which serve as cell-surface receptors of the Wnt pathway (*Fzd1*, *Fzd2*, *Fzd5*, *Fzd6*, *Fzd7*, *Fzd9*, *Fzd10*), and Wnt targets (*Axin2*, *CCND1*, *CD44*, and *EGFR*) in *Bves*$^{-/-}$ enteroids **(Figure 4C-E)**, suggesting that amplified Wnt signaling may contribute to these stemness phenotypes.

Given the amplified Wnt signaling at baseline in the *Bves*$^{-/-}$ enteroids, we next examined if they might be hyper-responsive to Wnt pathway stimulation or inhibition through media addition of Wnt3a or depletion of R-spondin, an amplifier of Wnt tone. *Bves*$^{-/-}$ enteroids were indeed hyper-responsive to Wnt stimulation, as evidenced by a higher percentage of stem-like cystic enteroids when stimulated with Wnt3a addition **(Figure 5A).** No significant differences in viability were observed on any given day post-plating between WT and *Bves*$^{-/-}$ enteroids with R-spondin depletion (**Figure 5B**).

As our prior studies have demonstrated that BVES expression directly correlates with E-cadherin expression, alters β-catenin subcellular localization, and inversely correlates with *ZEB1* expression in cancer cell lines[26], we hypothesized that the effects on Wnt signaling may be mediated via a direct BVES:E-cadherin interaction. We attempted to co-immunopurify BVES and E-cadherin, but did not detect evidence for complex formation between these two proteins (**Figure S3A**). Furthermore, review of a previously-conducted yeast-two-hybrid screen for BVES-interacting proteins did not identify E-cadherin, despite robust representation of E-cadherin in the library (Data not shown). However, consistent with our prior findings, we identified that E-cadherin expression is decreased in the *Bves*$^{-/-}$ small intestine relative to WT (**Figure S3B**), indicating that the previously-identified relationship between BVES and E-cadherin levels in cell culture models occurs *in vivo* and is not due to direct or indirect BVES:E-cadherin containing complexes.

Finally, we investigated if *Bves* expression varied between crypt and villus epithelial cell populations by quantifying *Bves* transcript levels in crypt and villus epithelial isolates. We noted an over 5-fold enrichment in its expression in the villus and

relatively low expression in the crypts **(Figure S4A)**. This corresponded to an 8-fold increased mRNA expression of *Lgr5* in the crypt versus villus isolates **(Figure S4B)**. This expression pattern is consistent with the stem cell phenotypes observed in the *Bves*$^{-/-}$ mice and enteroids. Collectively, these data identify a previously-unrecognized role for BVES in regulating stem cell dynamics of the small intestine and suggest that BVES may participate in a repression circuit that attenuates WNT signaling.

Intestinal *Bves* expression is downregulated after radiation and determines crypt viability.

Stem cell populations are critical to repopulating the intestinal epithelium after radiation injury to the small intestine[17,22]. As we observed that BVES regulates stem cell programs, we postulated that BVES would impact crypt regenerative dynamics after ionizing radiation[1,19]. We first determined if *Bves* expression is altered in response to radiation, and observed that 96 hours after 12 Gy WBR that *Bves* messenger RNA was reduced more than 2.5-fold **(Figure 6A)**. This time point is known to be one of intestinal crypt regeneration[10,33]. We then took advantage of the availability of the *Bves*$^{-/-}$ mice to test if the observed difference in *Bves* expression was functionally relevant to intestinal injury responses. WT and *Bves*$^{-/-}$ cohorts were exposed to 12 Gy radiation and sacrificed after 96 hours. Mice were injected with vincristine, a mitotic inhibitor, three hours prior to sacrifice to facilitate identification of regenerative crypts. Examination of hematoxylin and eosin (H&E) stained sections revealed that *Bves*$^{-/-}$ mice exhibited significantly greater crypt viability in comparison to WT mice after radiation exposure **(Figure 6B)**. Crypts were considered viable if three or more mitotic bodies were observed per crypt[19,32]. *Bves*$^{-/-}$ mice also exhibited significantly greater proliferation

(Figure 6C) but no differences in apoptosis **(Figure 6D)**. We investigated if this phenomenon was present in the colon, as well, but did not find significant differences in colonic crypt viability between the WT and *Bves*$^{-/-}$ cohorts **(Figure S5A-B)**. Taken together, these data suggest that BVES modulates small intestinal crypt viability after radiation and that its deletion promotes radioresistance.

BVES deletion results in amplified stem cell activity and Wnt signaling after radiation.

Surviving stem cells are critical to the repopulation of intestinal crypts after radiation, and we observed an expanded stem cell population in the *Bves*$^{-/-}$ mice at baseline. Therefore, we investigated if alterations in surviving stem cell populations after radiation may be contributing to the increased crypt viability in these mice. qRT-PCR analysis revealed increases in *Bmi1* and *TERT* **(Figure 7A)** in *Bves*$^{-/-}$ mice, as well as *Lgr5* and *Ascl2* **(Figure 7B).** Therefore, unlike mice at baseline, we observed significant upregulation of markers of both +4 damage-responsive and CBC intestinal stem cell populations. Moreover, as Wnt signaling is a key signaling pathway that governs intestinal homeostasis and regeneration after injury, and given the amplified Wnt signaling present in the *Bves*$^{-/-}$ intestine at baseline and in *ex vivo* cultures, we assessed if alterations in the Wnt pathway were present after radiation. qRT-PCR analysis revealed significant upregulation of several Wnt ligands (*Wnt1*, *Wnt2*, *Wnt2b*, *Wnt3*, *Wnt3a*, *Wnt6, Wnt7b*, *Wnt8b*, *Wnt9a*, *Wnt10b*, and *Wnt16*)**,** Frizzled receptors (*Fzd3*, *Fzd8*, *Fzd9*, and *Fzd10*), and Wnt targets genes (*Lgr5*, *Ascl2*, *Sox2*, *VegfA*) in the *Bves*$^{-/-}$ mice compared to WT **(Figure 7C-E)**. Thus, amplified Wnt signaling may

contribute to the increased proliferation and crypt viability observed in BVES knockout mice following radiation and supports stem cell survival and regeneration.

Bves$^{-/-}$ enteroids demonstrate radioresistance.

As we observed increased crypt viability *in vivo* after radiation of *Bves*$^{-/-}$ intestine, we hypothesized that *Bves*$^{-/-}$ enteroid plating efficiency, a surrogate marker for crypt viability, would be similarly impacted after radiation. We dosed mice with 12 Gy WBR, isolated SI tissue, and plated crypts 4 hours later. Consistent with our observations at the 96 hour time point, we observed no differences in apoptosis between the cohorts **(Figure S6A)**. However, we observed a 2-fold increase in *Bves*$^{-/-}$ enteroid plating efficiency 24 hours after plating **(Figure S6B)**. These data suggest an epithelial tissue-autonomous role for BVES in regulating intestinal crypt viability after radiation.

DISCUSSION

In this study, we investigated the role of BVES in intestinal homeostasis, stem cell function, and response to injury after ionizing radiation. At baseline, *Bves*$^{-/-}$ mice demonstrated altered lineage allocation, increased crypt size, and higher intestinal proliferation with an expanded intestinal stem cell population. *Bves*$^{-/-}$ enteroids exhibited increased stemness with increased plating efficiency, proportion of stem spheroids, retention of cystic structures, response to Wnt activation, as well as increased expression of both CBC and +4 stem cell populations. These *ex vivo* studies suggest that the altered stem cell dynamics in the *Bves*$^{-/-}$ intestine may not require stromal-epithelial crosstalk, thus identifying a previously unrecognized role for BVES in stem cell biology that is epithelial cell-autonomous. Moreover, we found that *Bves* expression was

downregulated in WT SI after radiation, and *Bves*$^{-/-}$ mice displayed significantly greater crypt viability after radiation. Additionally, the *Bves*$^{-/-}$ cohort demonstrated increased populations of both CBC and damage-responsive +4 stem cell populations after radiation, along with significantly amplified Wnt signaling. Lastly, *Bves*$^{-/-}$ crypts isolated from mice 4 hours after 12 Gy radiation displayed increased plating efficiency, thus demonstrating increased viability in an *ex vivo* setting, as well.

Peak apoptosis of the Lgr5^{+}-CBC stem cell population is thought to occur 4-6 hours after 12 Gy WBR[18,33]. After peak crypt loss between 48-72 hours after 12 Gy WBR, crypt regeneration actively occurs at 96 hours[18,33]. It is generally accepted that there are at least two subsets of stem cells: (1) a rapidly-cycling, CBC stem cell population at the base of the intestinal crypts, whose marker is Lgr5, a transmembrane receptor for R-spondin that amplifies Wnt tone, as well as Ascl2, Olfm4, Msi1, Smoc2, and Sox9; and (2) a damage-responsive, reserve stem cell population that is capable of repopulating the crypt and replacing Lgr5^{+}-CBC stem cells in case of injury to the small intestinal epithelium[1,5,9,11,22]. Markers for the latter subset of stem cells include Bmi1, TERT, as well as Lrig1 and Hopx[1,10]. While the role of Lgr5^{+}-CBC and +4 stem cell populations in repopulating intestinal crypts is under debate, studies have demonstrated that there is a role for each population in crypt regeneration[17,18,22]. While the +4 stem cell population is thought to be a more damage-responsive population that is capable of repopulating the crypt after injury[22], recent studies have shown that Lgr5^{+}-CBC stem cell populations are radioresistant and are critical to crypt regeneration after injury[17,18]. Interestingly, markers for both the CBC and the putative +4 damage-responsive populations were elevated in the BVES knockout mice, suggestive of either higher

proportions in survival of an already expanded stem cell population, or a more robust reparative mechanism driven by surviving stem cell populations.

While we observed an increase in crypt viability in the small intestine after radiation, this was not present in the colon. Given the variable radiosensitivities of the colon and small intestine, however, these findings were not unexpected[38–40]. A number of other groups have demonstrated varying radiosensitivities of the small and large intestine after radiation injury, which is impacted by factors such as the different rates of apoptosis in these tissues, and may be partially attributable to decreased p53 expression in the crypts of the colon compared to those in the small intestine[38–41].

Moreover, our findings of equivalent plating efficiencies after flow-sorting and plating WT and *Bves*$^{-/-}$ Lgr5^{+}-GFP^{+} cells indicates that the increased plating efficiency of intestinal crypts and persistence of cystic structures after BVES deletion may be dependent on stem cell interactions with other epithelial cell populations. Indeed, other intestinal epithelial populations such as Paneth cells are known to be critical to supporting intestinal stem cell populations at baseline and in response to radiation injury[1–3,17]. It is therefore possible that the phenotypes observed after BVES deletion may be a result of its absence in both stem cell and non-stem cell epithelial populations.

The Wnt signaling pathway is known to play a key role in the regulation of intestinal epithelial homeostasis as Wnt activation drives stem cell activity and maintains the intestinal stem cell niche[12,13,42]. Multiple studies have demonstrated that Wnt signaling is essential to mediating the survival of stem/progenitor cell populations after radiation[42–44]. We have previously demonstrated that BVES regulates Wnt signaling through E-cadherin stabilization and alterations in β-catenin distribution[26], but this is the

first study to directly link BVES to intestinal stem cell regulation *in vivo* and *ex vivo*. In support of BVES deletion altering intestinal stem cell function, baseline characterization of *Bves*$^{-/-}$ mice demonstrated elevated expression of *Lgr5* as well as an expanded stem cell compartment when crossed with the Lgr5-EGFP reporter line. *Bves*$^{-/-}$ crypts in the enteroid culture system demonstrated increased plating efficiency, proportions of stem spheroids, and enteroids with peripheral cystic structures, along with elevations in stem cell markers and Wnt ligands, receptors, and targets. Correspondingly, amplified Wnt signaling was also present in the *Bves*$^{-/-}$ intestine after radiation-induced injury, and may contribute to the increased crypt proliferation and viability observed after BVES deletion.

While we observed alterations in the Wnt pathway after BVES deletion, with impacts on intestinal stem cell dynamics and response to radiation injury, it is also possible that the observed phenotypes are being influenced by other signaling pathways. Indeed, we observed perturbations in Notch signaling in our enteroid platform after BVES deletion, with increased expression of *Atoh1*, consistent with our findings of an expanded goblet cell population in the small intestine and elevated *Muc2* expression in the enteroids. This was not present in the small intestinal tissue, however, suggesting a more pronounced suppression of global Notch signaling in an epithelial-autonomous setting after BVES deletion. Given that there is crosstalk between these pathways in maintaining the intestinal stem cell niche and in driving intestinal epithelial cell differentiation, it is possible that BVES influences stem cell, proliferative, and differentiation programs through alterations of both the Wnt and Notch pathways.

Moreover, studies have identified BVES as a regulator of a diverse group of pathways and cellular processes. We have previously shown that BVES alters cellular motility and cytoskeletal arrangement through its regulation of RhoA signaling[26,45]. Additionally, BVES was recently found to impact vesicular trafficking through its interaction with VAMP3, a SNARE protein that recycles transferrin and β1-integrin receptors[46]. As a protein originally discovered to play a role in cardiac development, BVES has also been shown to regulate a number of processes relevant to cardiac physiology. For example, BVES binds cAMP with high affinity, interacts with the potassium channel TREK-1, and regulates cardiac pacemaking[47]. Additionally, BVES interacts with the caveolin Cav3 to regulate the structural and functional integrity of caveolae in cardiac myocytes[48]. Thus, BVES impacts a number of cellular processes with broad physiological implications. Given the known prominent role of Wnt signaling in stem cell biology, however, we postulate that the phenotype of radioresistance described in this report is due to loss of BVES repression of Wnt signaling.

In conclusion, our findings demonstrate that BVES is critical for multiple aspects of small intestinal homeostasis and response to injury. Specifically, BVES regulates intestinal stem cell programs and is important in radiation-induced injury responses. This is the first study to identify that *Bves* is regulated in response to radiation, and that its underexpression has a clear biological impact on crypt regeneration, as the *Bves*$^{-/-}$ small intestine is protected from radiation injury. This study offers promise in understanding the molecular mechanisms that regulate response to radiation therapy and a potentially attractive target for predicting radiation response in patients undergoing radiotherapy.

ACKNOWLEDGEMENTS

The authors thank members of the Williams laboratory for thoughtful discussions about this research project. This work was supported by National Institutes of Health R01DK099204 and K08DK080221 to CSW, 1F30DK103498 and T32GM07347 to VKR, and P50CA095103 to MKW; P30DK058404 (Vanderbilt Digestive Disease Research Center); American Cancer Society Research Scholar Grants 116552 to CSW; Office of Medical Research, Department of Veterans Affairs (Merit Review Grant 1I01BX001426) to CSW; and Medical Research Council (MR/J010383/1) to TB. This publication was also supported in part by the National Cancer Institute Cancer Center Support Grant P30CA068485 and by CTSA award UL1TR000445 from the National Center for Advancing Translational Sciences. The content is solely the responsibility of the authors and does not necessarily represent the official views of the NIH.

FIGURE LEGENDS

Figure 1: BVES regulates intestinal proliferation, lineage allocation, and crypt morphology. Small intestines were isolated and Swiss-rolled. (A) Representative H&E staining of sections of WT and *Bves*$^{-/-}$ small intestine. Images (left) and quantification (right) of WT and *Bves*$^{-/-}$ villus height (358 μm vs. 364 μm, *P*=0.76) and crypt depth (80.4 μm vs. 98.0 μm, ***P*<0.01, n=24). (B) Images (left) and quantification (right) of apoptotic cells per crypt/villus unit (1.2 vs. 1.0 TUNEL^{+} cells/crypt-villus unit, *P*=0.37, n=24). (C) Images (left) and quantification (right) of crypt proliferation (6.0 vs. 7.5 phospho-Histone H3^{+} cells/crypt, ***P*<0.01, n=24). (D) Images (left) and quantification (right) of goblet cells/crypt-villus unit (13.1 vs. 20.2 PAS^{+} cells/crypt, ***P*<0.01, n=23). (E) Images (left) and quantification (right) of Paneth cells/crypt-villus unit (3.3 vs. 3.6 Lysozyme^{+} cells/crypt, *P*=0.39, n=19). (F) Images (left) and quantification (right) of enteroendocrine cells/crypt-villus unit (1.4 vs. 1.1 CgA^{+} cells/crypt, *P*=0.10, n=24). All images were captured at 100x magnification. Black arrows indicate positively-stained cells.

Figure 2: BVES regulates intestinal stem cell dynamics *in vivo*. (A) qRT-PCR analysis revealed increased expression of (A) *Axin2* (**P*<0.05, n=12) and (B) *Lgr5* (**P*<0.05, n=12) but no significant difference in mRNA levels of (C) *Lrig1* (*P*=0.21, n=12) and *Bmi1* (*P*=0.41, n=12) in *Bves*$^{-/-}$ proximal small intestine compared to WT. (D) Intercross of WT and *Bves*$^{-/-}$ mice with Lgr5-EGFP-ires-CreERT2 mice revealed increased number of GFP^{+} cells/$^{+}$crypt (3.5 vs. 5.2, ***P*<0.01, n=16) in the *Bves*$^{-/-}$ cohort. Images were captured at 400x magnification.

Figure 3: *Bves*$^{-/-}$ enteroids exhibit increased stemness *ex vivo*. Small intestinal crypts were isolated from WT or *Bves*$^{-/-}$ mice and embedded in Matrigel. (A) qRT-PCR analysis revealed increases in (A) *PCNA* (***P<0.001, n=6) and (B) *Muc2* (**P<0.01, n=6) mRNA levels in *Bves*$^{-/-}$ enteroids compared to WT. Enteroid stem cell properties determined based on (C) plating efficiency ratio, as measured by percentage of surviving enteroids 24 and 48 hours post-plating compared to total crypts plated (24 hours, **P<0.01; 48 hours, **P<0.01; n=6); (D) ratio of stem spheroid proportions counted 24 and 48 hours post-plating (24 hours, **P<0.01; 48 hours, **P<0.01; n=6) and (E) percentage of enteroids maintaining peripheral cystic structures 5 days after passaging (3.8 ± 1.0% vs. 10.2 ± 0.6%, **P<0.01, n=6). Images were captured at 40x magnification (3C) or 100x magnification (3D, 3E).

Figure 4: BVES regulates intestinal stem cell dynamics and Wnt signaling *ex vivo*. qRT-PCR analysis revealed increases in expression of **(**A) CBC stem cell markers in *Bves*$^{-/-}$ enteroids compared to WT. *Lgr5*, *Ascl2*, *Olfm4*, *Nanog*, and *Sox9* mRNA levels in *Bves*$^{-/-}$ enteroids compared to WT. qRT-PCR analysis also revealed increases in (B) +4 stem cell markers *Bmi1* and *Lrig1* mRNA levels in *Bves*$^{-/-}$ enteroids compared to WT with no significant differences in *TERT* expression (P=0.11). Expression of (C) Wnt ligands, (D) Wnt receptors, and (E) Wnt targets were significantly elevated in the *Bves*$^{-/-}$ enteroids. *P<0.05, **P<0.01 (n=6).

Figure 5: *Bves*$^{-/-}$ enteroids are hyper-responsive to Wnt activation. (A) *Bves*$^{-/-}$ enteroids were hyper-responsive to Wnt activation, with a significantly higher percentage of cystic enteroids present on days 1-5 post-plating after Wnt3a addition to growth factor media. Representative images of enteroids on day 6 post-plating are

shown below at 40x (left) and 100x (right) magnification. Cystic structures are marked by arrowheads. (B) No significant differences were observed in WT and *Bves*$^{-/-}$ enteroid viability on any given day post-plating with R-spondin growth factor depletion. **P*<0.05, ***P*<0.01 (n=6).

Figure 6: BVES regulates intestinal crypt viability after radiation. (A) qRT-PCR analysis comparing *Bves* mRNA expression in WT proximal small intestine prior to radiation vs. 4 hours (*P*=0.30, n=12), and 96 hours after 12 Gy radiation (**P*=0.05, n=12). (B) Representative H&E stained sections and quantification of viable intestinal crypts in WT and *Bves*$^{-/-}$ mice. *Bves*$^{-/-}$ mice exhibited significantly greater crypt viability 96 hours after 12 Gy radiation (42.5 ± 7.8% vs. 64.4 ± 3.7% **P*<0.05, n=17). Crypts were considered viable if 3 or more mitotic bodies were observed per crypt. 40 sequential, well-aligned crypts in the proximal one-third of the small intestine were counted per data point. The percent of surviving crypts was calculated using the following equation: (# of viable crypts/total # of crypts counted) x 100. (C) Images (left) and quantification (right) of crypt proliferation 96 hours after 12 Gy radiation (14.4 vs. 20.0 phospho-Histone H3^{+} cells/crypt, **P*<0.05, n=17). (D) Images (left) and quantification (right) of apoptotic cells per crypt/villus unit (4.1 vs. 4.3 TUNEL^{+} cells/crypt-villus unit, *P*=0.79, n=17). Images were captured at 10x magnification (5B, left) or 100x magnification (5B, right, 5C, 5D).

Figure 7: BVES modulates stem cell regenerative responses and Wnt signaling after radiation. Proximal small intestine was harvested from WT or *Bves*$^{-/-}$ mice after 12 Gy WBR. qRT-PCR analysis revealed increases in mRNA expression of (A) +4 stem cell markers *Bmi1* and *TERT* and (B) CBC stem cell markers *Lgr5* and *Ascl2* in *Bves*$^{-/-}$

proximal SI compared to WT. Expression of (C) Wnt ligands, (D) Wnt receptors, and (E) Wnt targets was significantly elevated in the *Bves*$^{-/-}$ proximal SI compared to WT. (*P<0.05, **P<0.01, n=12)

Supplemental Figure 1: Magnification of WT and *Bves*$^{-/-}$ small intestine. Left to Right: TUNEL staining for apoptotic cells, pH3 staining for proliferating cells, PAS staining for goblet cells, lysozyme staining for Paneth cells, and CgA staining for enteroendocrine cells. Black arrows indicate positively-stained cells.

Supplemental Figure 2: *Bves*$^{-/-}$ enteroids demonstrate altered lineage allocation and Notch signaling. qRT-PCR analysis revealed significantly higher mRNA expression of (A) *Spedf*, a secretory lineage marker, along with (B) Notch target *Atoh1* in the *Bves*$^{-/-}$ enteroids compared to WT but (C) no significant differences in their expression or other Notch pathway genes in small intestinal tissue (*P<0.05, n=12).

Supplemental Figure 3: **BVES and E-cadherin do not interact in a complex.** (A) E-cadherin does not co-immunoprecipitate with BVES in human corneal epithelial cell (HCE) lines. (B) E-cadherin expression was decreased in the *Bves*$^{-/-}$ small intestine compared to WT small intestine.

Supplemental Figure 4: *Bves* is highly expressed in small intestinal villi with relatively low expression in intestinal crypts. qRT-PCR analysis comparing (A) *Bves* and (B) *Lgr5* mRNA expression in WT proximal small intestine crypt and villus isolates (*P<0.05, **P<0.01, n=6).

Supplemental Figure 5: BVES deletion does not impact colonic crypt viability. (A) Representative H&E stained sections of WT and *Bves*$^{-/-}$ colons 96 hours after 12 Gy

radiation. (B) No significant differences in colonic crypt viability were observed (*P*=0.59, n=17). Crypts were considered viable if 3 or more mitotic bodies were observed per crypt. 40 sequential, well-aligned crypts in the distal one-third of the colon were counted per mouse. The percent of surviving crypts was calculated using the following equation: (# of viable crypts/total # of crypts counted) x 100.

Supplemental Figure 6: BVES deletion protects intestinal crypts after radiation. (A) Quantification of apoptotic cells per crypt/villus unit (10.5 vs. 10.5 $TUNEL^+$ cells/crypt-villus unit, *P*=0.97, n=19) in WT and $Bves^{-/-}$ proximal SI 4 hours after 12 Gy radiation. (B) Enteroids harvested from $Bves^{-/-}$ mice after 12 Gy radiation demonstrated increased plating efficiency when compared to WT (***P*<0.01, n=6).

REFERENCES

1. Barker, N. Adult intestinal stem cells: critical drivers of epithelial homeostasis and regeneration. *Nat. Rev. Mol. Cell Biol.* **15,** 19–33 (2014).

2. Sato & Clevers, H. Growing self-organizing mini-guts from a single intestinal stem cell: mechanism and applications. *Science* **340,** 1190–4 (2013).

3. Clevers, H. The intestinal crypt, a prototype stem cell compartment. *Cell* **154,** 274–84 (2013).

4. Barker, N., van de Wetering, M. & Clevers, H. The intestinal stem cell. *Genes Dev.* **22,** 1856–64 (2008).

5. Potten, Gandara, R., Mahida, Y. R., Loeffler, M. & Wright, N. a. The stem cells of small intestinal crypts: where are they? *Cell Prolif.* **42,** 731–50 (2009).

6. Sato, T. *et al.* Single Lgr5 stem cells build crypt-villus structures in vitro without a mesenchymal niche. *Nature* **459,** 262–5 (2009).

7. Sato, T. *et al.* Paneth cells constitute the niche for Lgr5 stem cells in intestinal crypts. *Nature* **469,** 415–8 (2011).

8. Barker, N. *et al.* Identification of stem cells in small intestine and colon by marker gene Lgr5. *Nature* **449,** 1003–7 (2007).

9. Li & Clevers, H. Coexistence of quiescent and active adult stem cells in mammals. *Science* **327,** 542–545 (2010).

10. Van Landeghem, L. *et al.* Activation of two distinct Sox9-EGFP-expressing intestinal stem cell populations during crypt regeneration after irradiation. *Am. J. Physiol. Gastrointest. Liver Physiol.* **302,** G1111–32 (2012).

11. Durand, A. *et al.* Functional intestinal stem cells after Paneth cell ablation induced by the loss of transcription factor Math1 (Atoh1). *Proc. Natl. Acad. Sci.* **109,** 8965–8970 (2012).

12. Pinto, D., Gregorieff, A., Begthel, H. & Clevers, H. Canonical Wnt signals are essential for homeostasis of the intestinal epithelium. *Genes Dev.* 1709–1713 (2003).

13. Gregorieff, A. & Clevers, H. Wnt signaling in the intestinal epithelium: from endoderm to cancer. *Genes Dev.* **19,** 877–90 (2005).

14. Van Es, J. H. *et al.* A critical role for the Wnt effector Tcf4 in adult intestinal homeostatic self-renewal. *Mol. Cell. Biol.* **32,** 1918–27 (2012).

15. Clevers, H. & Nusse, R. Wnt/β-catenin signaling and disease. *Cell* **149,** 1192–1205 (2012).

16. Bray, S. J. Notch signalling: a simple pathway becomes complex. *Nat. Rev. Mol. Cell Biol.* **7,** 678–689 (2006).

17. Metcalfe, C., Kljavin, N. M., Ybarra, R. & De Sauvage, F. J. Lgr5+ stem cells are indispensable for radiation-induced intestinal regeneration. *Cell Stem Cell* **14,** 149–159 (2014).

18. Hua, G. *et al.* Crypt base columnar stem cells in small intestines of mice are radioresistant. *Gastroenterology* **143,** 1266–76 (2012).

19. Ottewell, P. D. *et al.* Gastrin increases murine intestinal crypt regeneration following injury. *Gastroenterology* **130,** 1169–80 (2006).

20. Potten, Booth, C. & Pritchard, D. M. Stem Cell Review The intestinal epithelial stem cell : the mucosal governor. 219–243 (1997).

21. Booth, C. & Potten, C. S. Gut instincts: thoughts on intestinal epithelial stem cells. *J. Clin. Invest.* **105,** 1493–9 (2000).

22. Tian, H. *et al.* A reserve stem cell population in small intestine renders Lgr5-positive cells dispensable. *Nature* **478,** 255–9 (2011).

23. Buczacki, S. J. a *et al.* Intestinal label-retaining cells are secretory precursors expressing Lgr5. *Nature* **495,** 65–9 (2013).

24. Reese, D., Zavaljevski, M., Streiff, N. & Bader, D. Bves: A Novel Gene Expressed during Coronary Blood Vessel Development. *Dev. Biol.* **209,** 159–71 (1999).

25. Andrée, B. *et al.* Isolation and characterization of the novel popeye gene family expressed in skeletal muscle and heart. *Dev. Biol.* **223,** 371–82 (2000).

26. Williams, C. S. *et al.* BVES regulates EMT in human corneal and colon cancer cells and is silenced via promoter methylation in human colorectal carcinoma. *J. Clin. Invest.* **121,** 4056–4069 (2011).

27. Andrée, Fleige, A., Arnold, H. & Brand, T. Mouse Pop1 Is Required for Muscle Regeneration in Adult Skeletal Muscle. *Mol. Cell. Biol.* **22,** 1504–12 (2002).

28. Kawaguchi, M. *et al.* Identification of a novel intracellular interaction domain essential for Bves function. *PLoS One* **3,** e2261 (2008).

29. Vasavada, T. K., DiAngelo, J. R. & Duncan, M. K. Developmental Expression of Pop1/Bves. *J. Histochem. Cytochem.* **52,** 371–377 (2004).

30. Jayagopal, A., Yang, J. L., Haselton, F. R. & Chang, M. S. Tight junction-associated signaling pathways modulate cell proliferation in uveal melanoma. *Investig. Ophthalmol. Vis. Sci.* **52,** 588–593 (2011).

31. Han, P. *et al.* BVES inhibition triggers epithelial-mesenchymal transition in human hepatocellular carcinoma. *Dig. Dis. Sci.* **59,** 992–1000 (2014).

32. Poindexter, S. V *et al.* Transcriptional co-repressor MTG16 regulates small intestinal crypt proliferation and crypt regeneration after radiation-induced injury. *Am. J. Physiol. - Gastrointest. Liver Physiol.* (2015).

33. Lund, P. K. Fixing the breaks in intestinal stem cells after radiation: a matter of DNA damage and death or DNA repair and regeneration. *Gastroenterology* **143,** 1144–7 (2012).

34. Mahe, M. M. *et al.* Establishment of Gastrointestinal Epithelial Organoids. *Curr Protoc Mouse Biol.* **3,** 217–240 (2013).

35. Barrett, C. W. *et al.* Dietary selenium deficiency exacerbates DSS-induced epithelial injury and AOM/DSS-induced tumorigenesis. *PLoS One* **8,** e67845 (2013).

36. Barrett, C. W. *et al.* Selenoprotein P influences colitis-induced tumorigenesis by mediating stemness and oxidative damage. *J. Clin. Invest.* **125,** 2646–2660 (2015).

37. Farin, H. F., Van Es, J. H. & Clevers, H. Redundant sources of Wnt regulate intestinal stem cells and promote formation of paneth cells. *Gastroenterology* **143,** 1518–1529.e7 (2012).

38. Gudkov, A. V & Komarova, E. a. The role of p53 in determining sensitivity to radiotherapy. *Nat. Rev. Cancer* **3,** 117–29 (2003).

39. Potten, C. S. & Grant, H. K. The relationship between ionizing radiation-induced apoptosis and stem cells in the small and large intestine. *Br. J. Cancer* **78,** 993–1003 (1998).

40. Cai, W. B., Roberts, S. A., Bowley, E., Hendry, J. H. & Potten, C. S. Differential survival of murine small and large intestinal crypts following ionizing radiation. *Int. J. Radiat. Biol.* **71,** 145–55 (1997).

41. Hendry, J. H., Cai, W. B., Roberts, S. A. & Potten, C. S. p53 deficiency sensitizes clonogenic cells to irradiation in the large but not the small intestine. *Radiat. Res.* **148,** 254–9 (1997).

42. Fevr, T., Robine, S., Louvard, D. & Huelsken, J. Wnt/beta-catenin is essential for intestinal homeostasis and maintenance of intestinal stem cells. *Mol. Cell. Biol.* **27,** 7551–9 (2007).

43. Kim, Y. *et al.* Wnt activation is implicated in glioblastoma radioresistance. *Lab. Invest.* **92,** 466–73 (2012).

44. Woodward, W. a *et al.* WNT/beta-catenin mediates radiation resistance of mouse mammary progenitor cells. *Proc. Natl. Acad. Sci. U. S. A.* **104,** 618–23 (2007).

45. Russ, P. K. *et al.* Bves modulates tight junction associated signaling. *PLoS One* **6,** e14563 (2011).

46. Hager, H., Roberts, R. J., Cross, E. E., Proux-Gillardeaux, V. & Bader, D. M. Identification of a novel Bves function: regulation of vesicular transport. *EMBO J.* **29,** 532–45 (2010).

47. Froese, A. *et al.* Popeye domain containing proteins are essential for stress-mediated modulation of cardiac pacemaking in mice. *J. Clin. Invest.* **122,** 1119–1130 (2012).

48. Alcalay, Y. *et al.* Popeye Domain Containing 1 (Popdc1/Bves) Is a Caveolae-Associated Protein Involved in Ischemia Tolerance. *PLoS One* **8,** e71100 (2013).

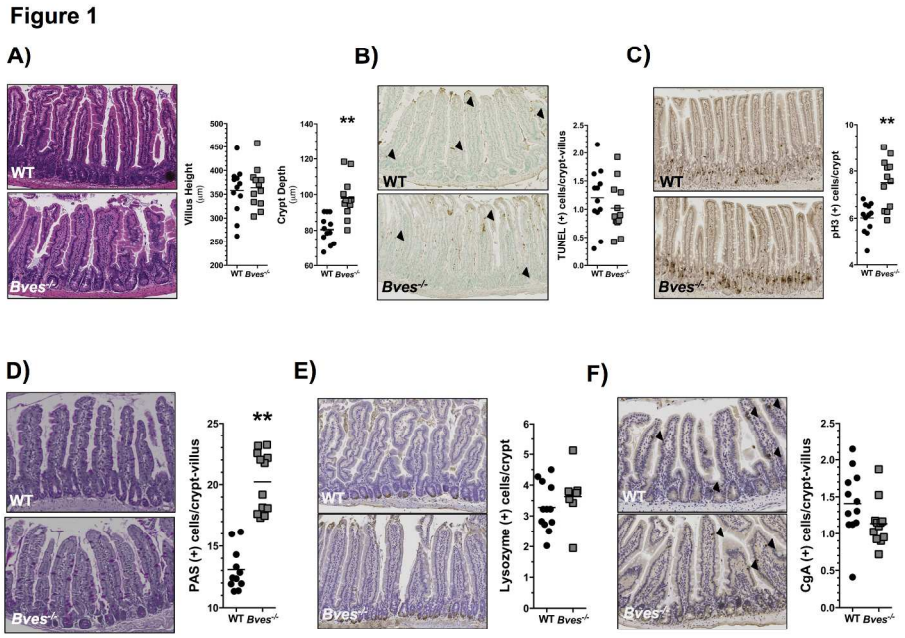

Figure 1: BVES regulates intestinal proliferation, lineage allocation, and crypt morphology. Small intestines were isolated and Swiss-rolled. (A) Representative H&E staining of sections of WT and *Bves*$^{-/-}$ small intestine. Images (left) and quantification (right) of WT and *Bves*$^{-/-}$ villus height (358 μm vs. 364 μm, P=0.76) and crypt depth (80.4 μm vs. 98.0 μm, **P<0.01, n=24). (B) Images (left) and quantification (right) of apoptotic cells per crypt/villus unit (1.2 vs. 1.0 TUNEL^{+} cells/crypt-villus unit P=0.37, n=24). (C) Images (left) and quantification (right) of crypt proliferation (6.0 vs. 7.5 phospho-Histone H3^{+} cells/crypt, **P<0.01, n=24). (D) Images (left) and quantification (right) of goblet cells/crypt-villus unit (13.1 vs. 20.2 PAS^{+} cells/crypt, **P<0.01, n=23). (E) Images (left) and quantification (right) of Paneth cells/crypt-villus unit (3.3 vs. 3.6 Lysozyme^{+} cells/crypt, P=0.39, n=19). (F) Images (left) and quantification (right) of enteroendocrine cells/crypt-villus unit (1.4 vs. 1.1 CgA^{+} cells/crypt, P=0.10, n=24). All images were captured at 100x magnification. Black arrows indicate positively-stained cells.
279x215mm (300 x 300 DPI)

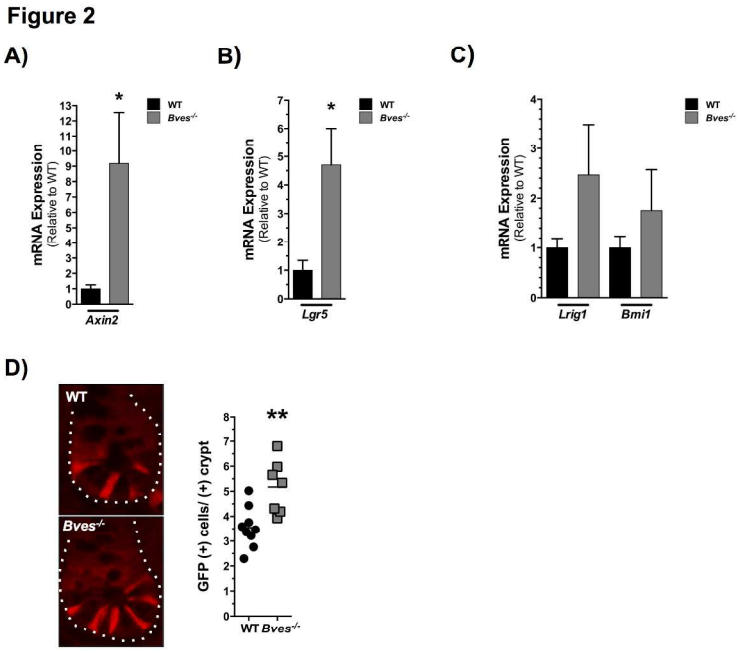

Figure 2: BVES regulates intestinal stem cell dynamics *in vivo*. (A) qRT-PCR analysis revealed increased expression of (A) *Axin2* (**P*<0.05, n=12) and (B) *Lgr5* (**P*<0.05, n=12) but no significant difference in mRNA levels of (C) *Lrig1* (*P*=0.21, n=12) and *Bmi1* (*P*=0.41, n=12) in *Bves*$^{-/-}$ proximal small intestine compared to WT. (D) Intercross of WT and *Bves*$^{-/-}$ mice with Lgr5-EGFP-ires-CreERT2 mice revealed increased number of GFP^{+} cells/$^{+}$crypt (3.5 vs. 5.2, ***P*<0.01, n=16) in the *Bves*$^{-/-}$ cohort. Images were captured at 400x magnification.
279x215mm (300 x 300 DPI)

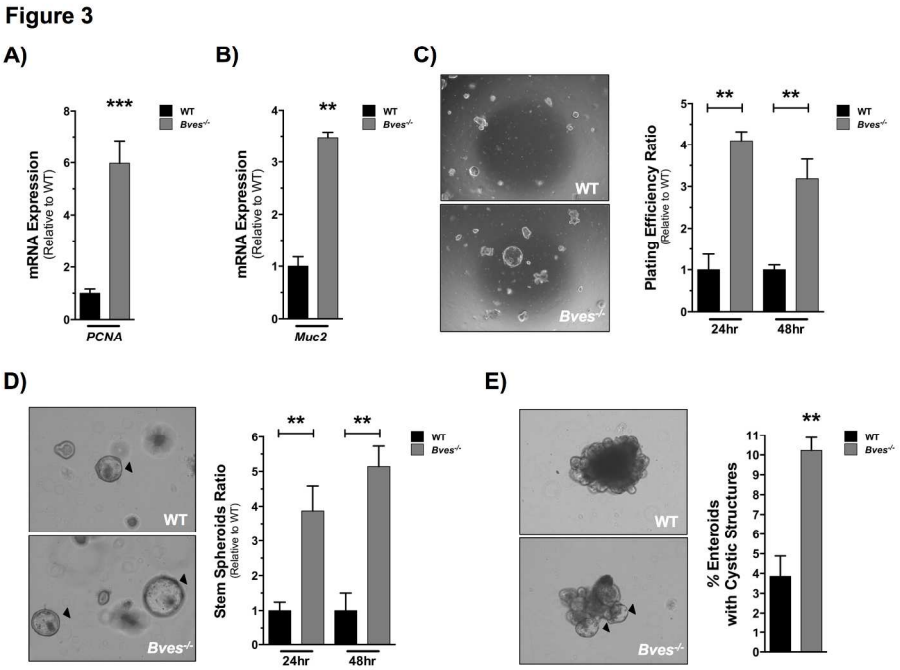

Figure 3: *Bves*$^{-/-}$ enteroids exhibit increased stemness *ex vivo*. Small intestinal crypts were isolated from WT or *Bves*$^{-/-}$ mice and embedded in Matrigel. (A) qRT-PCR analysis revealed increases in (A) *PCNA* (***P<0.001, n=6) and (B) *Muc2* (**P<0.01, n=6) mRNA levels in *Bves*$^{-/-}$ enteroids compared to WT. Enteroid stem cell properties determined based on (C) plating efficiency ratio, as measured by percentage of surviving enteroids 24 and 48 hours post-plating compared to total crypts plated (24 hours, **P<0.01; 48 hours, **P<0.01; n=6); (D) ratio of stem spheroid proportions counted 24 and 48 hours post-plating (24 hours, **P<0.01; 48 hours, **P<0.01; n=6) and (E) percentage of enteroids maintaining peripheral cystic structures 5 days after passaging (3.8 ± 1.0% vs. 10.2 ± 0.6%, **P<0.01, n=6). Images were captured at 40x magnification (3C) or 100x magnification (3D, 3E).
279x215mm (250 x 250 DPI)

Figure 4

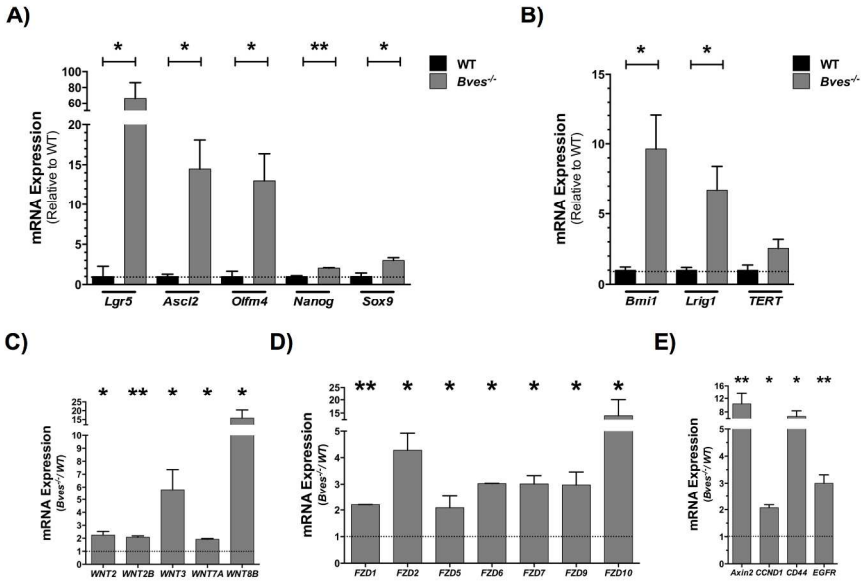

Figure 4: BVES regulates intestinal stem cell dynamics and Wnt signaling *ex vivo*. qRT-PCR analysis revealed increases in expression of (A) CBC stem cell markers in *Bves*$^{-/-}$ enteroids compared to WT. *Lgr5*, *Ascl2*, *Olfm4*, *Nanog*, and *Sox9* mRNA levels in *Bves*$^{-/-}$ enteroids compared to WT. qRT-PCR analysis also revealed increases in (B) +4 stem cell markers *Bmi1* and *Lrig1* mRNA levels in *Bves*$^{-/-}$ enteroids compared to WT with no significant differences in *TERT* expression (P=0.11). Expression of (C) Wnt ligands, (D) Wnt receptors, and (E) Wnt targets were significantly elevated in the *Bves*$^{-/-}$ enteroids. *P<0.05, **P<0.01 (n=6).
279x215mm (250 x 250 DPI)

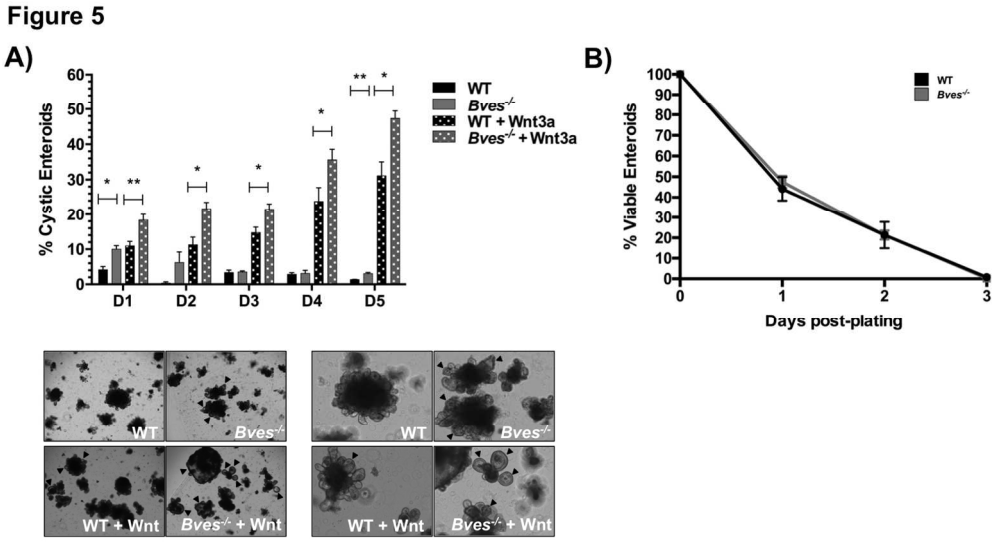

Figure 5: *Bves*$^{-/-}$ enteroids are hyper-responsive to Wnt activation. (A) *Bves*$^{-/-}$ enteroids were hyper-responsive to Wnt activation, with a significantly higher percentage of cystic enteroids present on days 1-5 post-plating after Wnt3a addition to growth factor media. Representative images of enteroids on day 6 post-plating are shown below at 40x (left) and 100x (right) magnification. Cystic structures are marked by arrowheads. (B) No significant differences were observed in WT and *Bves*$^{-/-}$ enteroid viability on any given day post-plating with R-spondin growth factor depletion. **P*<0.05, ***P*<0.01 (n=6).
564x423mm (72 x 72 DPI)

Figure 6

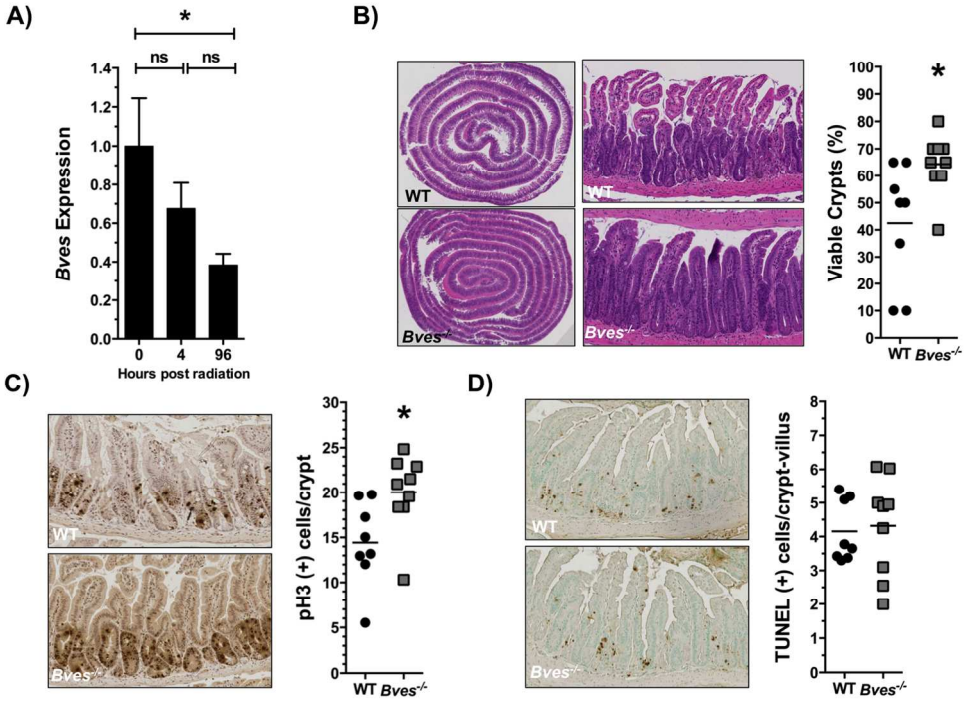

Figure 6: BVES regulates intestinal crypt viability after radiation. (A) qRT-PCR analysis comparing *Bves* mRNA expression in WT proximal small intestine prior to radiation vs. 4 hours (P=0.30, n=12), and 96 hours after 12 Gy radiation (*P=0.05, n=12). (B) Representative H&E stained sections and quantification of viable intestinal crypts in WT and *Bves*$^{-/-}$ mice. *Bves*$^{-/-}$ mice exhibited significantly greater crypt viability 96 hours after 12 Gy radiation (42.5 ± 7.8% vs. 64.4 ± 3.7% *P<0.05, n=17). Crypts were considered viable if 3 or more mitotic bodies were observed per crypt. 40 sequential, well-aligned crypts in the proximal one-third of the small intestine were counted per data point. The percent of surviving crypts was calculated using the following equation: (# of viable crypts/total # of crypts counted) x 100. (C) Images (left) and quantification (right) of crypt proliferation 96 hours after 12 Gy radiation (14.4 vs. 20.0 phospho-Histone H3^{+} cells/crypt, *P<0.05, n=17). (D) Images (left) and quantification (right) of apoptotic cells per crypt/villus unit (4.1 vs. 4.3 TUNEL^{+} cells/crypt-villus unit, P=0.79, n=17). Images were captured at 10x magnification (6B, left) or 100x magnification (6B, right, 6C, 6D).
564x423mm (72 x 72 DPI)

Figure 7

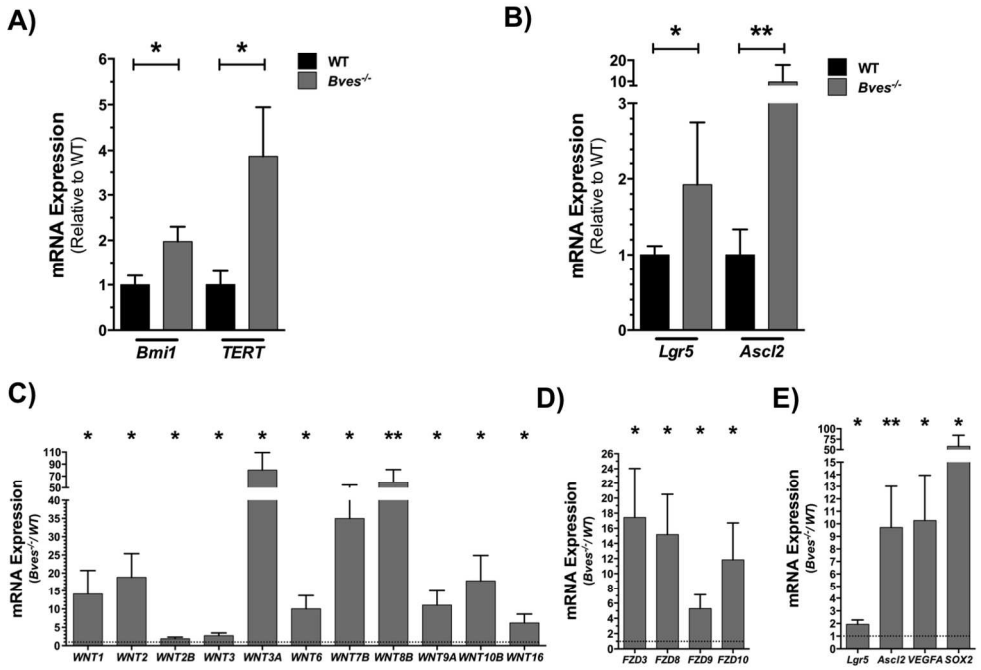

Figure 7: BVES modulates stem cell regenerative responses and Wnt signaling after radiation. Proximal small intestine was harvested from WT or *Bves*$^{-/-}$ mice after 12 Gy WBR. qRT-PCR analysis revealed increases in mRNA expression of (A) +4 stem cell markers *Bmi1* and *TERT* and (B) CBC stem cell markers *Lgr5* and *Ascl2* in *Bves*$^{-/-}$ proximal SI compared to WT. Expression of (C) Wnt ligands, (D) Wnt receptors, and (E) Wnt targets was significantly elevated in the *Bves*$^{-/-}$ proximal SI compared to WT. (*P<0.05, **P<0.01, n=12)
564x423mm (72 x 72 DPI)

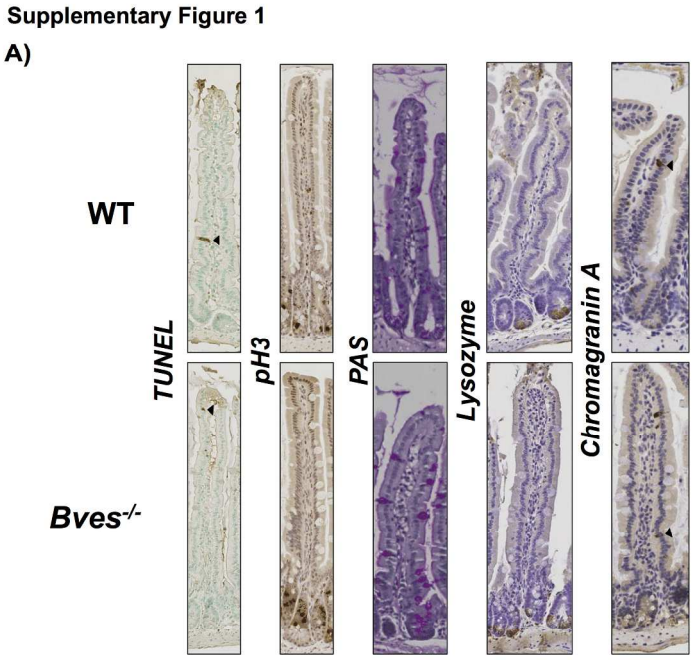

Supplemental Figure 1: Magnification of WT and *Bves*$^{-/-}$ small intestine. Left to Right: TUNEL staining for apoptotic cells, pH3 staining for proliferating cells, PAS staining for goblet cells, lysozyme staining for Paneth cells, and Cga staining for enteroendocrine cells. Black arrows indicate positively-stained cells.
279x215mm (250 x 250 DPI)

Supplementary Figure 2

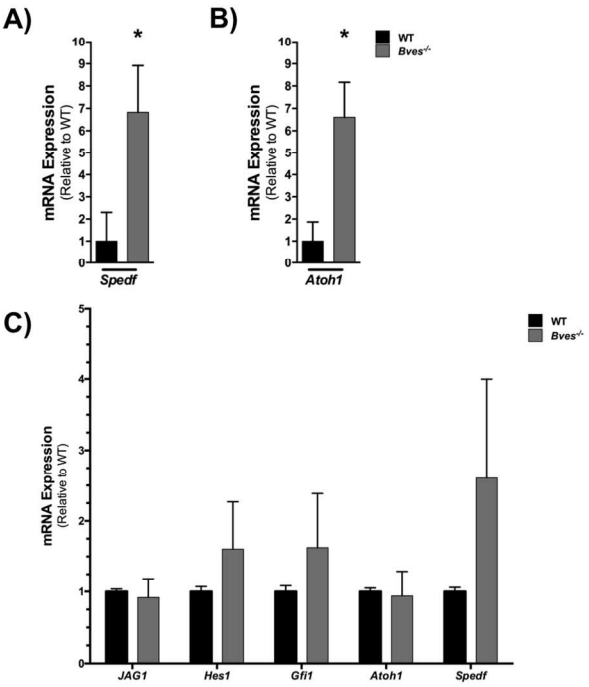

Supplemental Figure 2: *Bves*$^{-/-}$ enteroids demonstrate altered lineage allocation and Notch signaling. qRT-PCR analysis revealed significantly higher mRNA expression of (A) *Spedf*, a secretory lineage marker, along with (B) Notch target *Atoh1* in the *Bves*$^{-/-}$ enteroids compared to WT but (C) no significant differences in their expression or other Notch pathway genes in small intestinal tissue (*P<0.05, n=12). 564x423mm (72 x 72 DPI)

Supplementary Figure 3

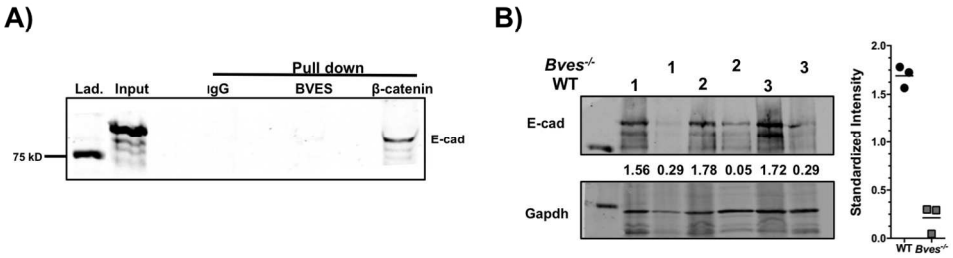

Supplemental Figure 3: BVES and E-cadherin do not interact in a complex. (A) E-cadherin does not co-immunoprecipitate with BVES in human corneal epithelial cell (HCE) lines. (B) E-cadherin expression was decreased in the *Bves*$^{-/-}$ small intestine compared to WT small intestine.
564x423mm (72 x 72 DPI)

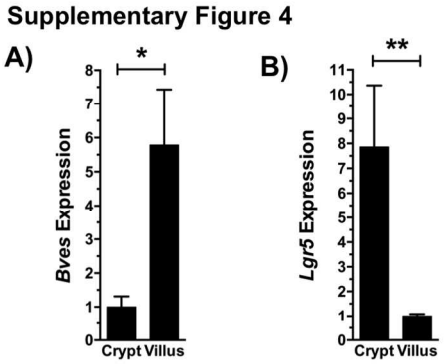

Supplemental Figure 4: *Bves* is highly expressed in small intestinal villi with relatively low expression in intestinal crypts. qRT-PCR analysis comparing (A) *Bves* and (B) *Lgr5* mRNA expression in WT proximal small intestine crypt and villus isolates (*P<0.05, **P<0.01, n=6).
564x423mm (72 x 72 DPI)

Supplementary Figure 5

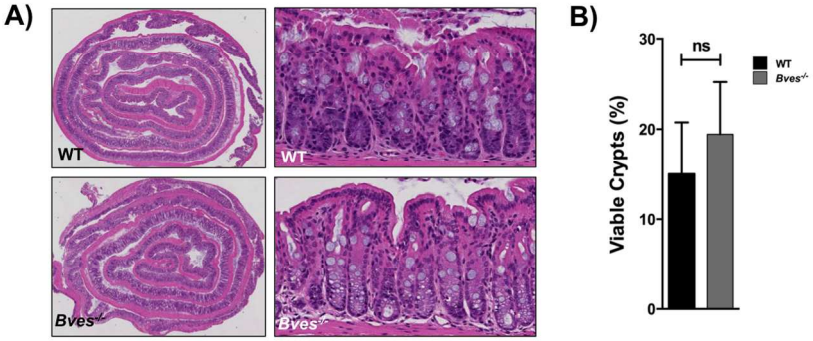

Supplemental Figure 5: BVES deletion does not impact colonic crypt viability. (A) Representative H&E stained sections of WT and *Bves*$^{-/-}$ colons 96 hours after 12 Gy radiation. (B) No significant differences in colonic crypt viability were observed (P=0.59, n=17). Crypts were considered viable if 3 or more mitotic bodies were observed per crypt. 40 sequential, well-aligned crypts in the distal one-third of the colon were counted per mouse. The percent of surviving crypts was calculated using the following equation: (# of viable crypts/total # of crypts counted) x 100.
564x423mm (72 x 72 DPI)

Supplementary Figure 6

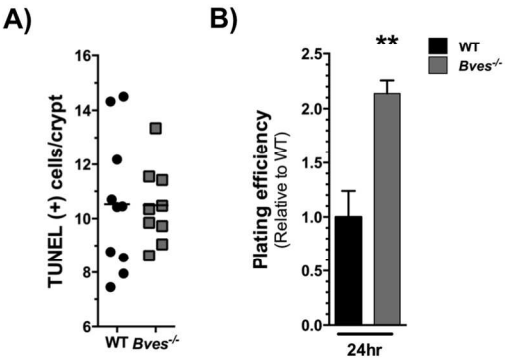

Supplemental Figure 6: BVES deletion protects intestinal crypts after radiation. (A) Quantification of apoptotic cells per crypt/villus unit (10.5 vs. 10.5 TUNEL^{+} cells/crypt-villus unit, P=0.97, n=19) in WT and *Bves*$^{-/-}$ proximal SI 4 hours after 12 Gy radiation. (B) Enteroids harvested from *Bves*$^{-/-}$ mice after 12 Gy radiation demonstrated increased plating efficiency when compared to WT (**P<0.01).
564x423mm (72 x 72 DPI)